HIGH-RESOLUTION POLARIMETRIC OBSERVATIONS OF AN EF-4 TORNADO ON 10 MAY 2010 FROM OU-PRIME

David Bodine[1,2,*], Matthew. R. Kumjian[1,2,3], Adam J. Smith[1,2], Robert D. Palmer[1,2], Alexander V. Ryzhkov[2,3], and Pamela L. Heinselman[4]

[1] School of Meteorology, The University of Oklahoma, Norman, OK, U.S.A.
[2] Atmospheric Radar Research Center, The University of Oklahoma, Norman, OK, U.S.A
[3] Cooperative Institute for Mesoscale Meteorological Studies, The University of Oklahoma, Norman, OK, U.S.A
[4] NOAA/OAR National Severe Storms Laboratory, Norman, OK, U.S.A

1. INTRODUCTION

Dual-polarization radar provides the capability to discriminate between meteorological and nonmeteorological scatterers (Zrnić and Ryzhkov, 1999), which has an important application for tornado detection. Owing to the random orientations, irregular shapes, high dielectric factors, and large sizes, lofted debris elements in a tornado produce a unique polarimetric signature called a tornadic debris signature (TDS; Ryzkhov et al., 2002). These scattering characteristics produce a distinct TDS characterized by high horizontal radar reflectivity factor (Z_{HH}), low differential reflectivity (Z_{DR}), and very low copolar cross-correlation coefficient (ρ_{HV}) values, which are typically collocated with the tornadic vortex signature at the tip of the hook echo.

In an examination of multiple tornado cases in central Oklahoma, Ryzhkov et al. (2005) showed that TDSs identified the locations of tornadoes of EF-3 strength or higher using S-band radars. Their study determined a preliminary criteria for tornado detection of $Z_{HH} > 45$ dBZ, $Z_{DR} < 0.5$ dB, and $\rho_{HV} < 0.8$. Ryzhkov et al. (2005) also showed that the minimum and average values of Z_{DR} and ρ_{HV} reached a minimum during periods of peak damage intensity for three different tornado cases. Bluestein et al. (2007) used a X-band, polarimetric radar to observe a TDS associated with a weak tornado, and found that precipitation may cause Z_{DR} values to exceed 0.5 dB. Nonetheless, very low ρ_{HV} values were observed within the tornado, suggesting that ρ_{HV} may provide the best indication of lofted tornadic debris. Kumjian and Ryzhkov (2008) examined TDSs associated with multiple tornadoes of EF-1 intensity or higher at S-band and C-band, provided they loft sufficient debris. Although, they also noted that some weak tornadoes may not loft sufficient debris to produce a TDS.

In addition to providing remote tornado detection capabilities, dual-polarization radar offers the opportunity to observe changes in the debris field of the tornado. As tornado intensity increases, the amount of debris lofted by the tornado likely increases, assuming other factors influencing tornado debris concentration stay relatively similar. Other factors, such as differences in debris concentration and type of debris element, may change significantly along the tornado's path (e.g., rural vs. urban areas). A more intense tornado may loft larger debris elements which may result in higher Z_{HH} and lower ρ_{HV}. Hence, dual-polarization radar may provide an opportunity to remotely observe changes in tornado intensity based on the changes in the tornado debris field. In this study, we investigate the evolution of the debris field of the Moore, Oklahoma EF-4 tornado on 10 May 2010 to determine if polarimetric radar can be used to determine damage intensity. Several TDS parameters are developed to provide a metric of tornado damage intensity. Such parameters may provide a set of tools for nowcasting changes in tornado intensity and remotely determining damage intensity.

* *Corresponding author address:* David Bodine, University of Oklahoma, School of Meteorology, 120 David L. Boren Blvd., Rm 4630, Norman, OK 73072-7307; e-mail: bodine@ou.edu

2. BACKGROUND

Observational and modeling studies have uncovered much information about tornado structure and debris patterns within tornadoes. For an extensive review on tornadoes, see Rotunno (1986), Church et al. (1993), and Davies-Jones et al. (2001). In this section, a brief review of tornado structure and debris characteristics relevant to this study is provided.

2.1. Tornado vortex structure

Tornado simulators provide a controlled environment to vary parameters such as circulation strength and updraft intensity (Ward, 1972; Davies-Jones, 1973; Church et al., 1979; Davies-Jones, 1986; Church and Snow, 1993). Such studies discovered the importance of the ratio of the magnitude of the circulation to the strength of the updraft, called the swirl ratio, to vortex state (Rotunno, 1977, 1979, 1984; Davies-Jones, 1986). As the swirl ratio increases, the structure of the tornado vortex evolves through several vortex states: i) a single-cell vortex, ii) a vortex breakdown with a single-cell vortex near the surface and a two-cell vortex aloft, iii) a two-cell vortex, iv) and multiple vortices (Davies-Jones, 1986).

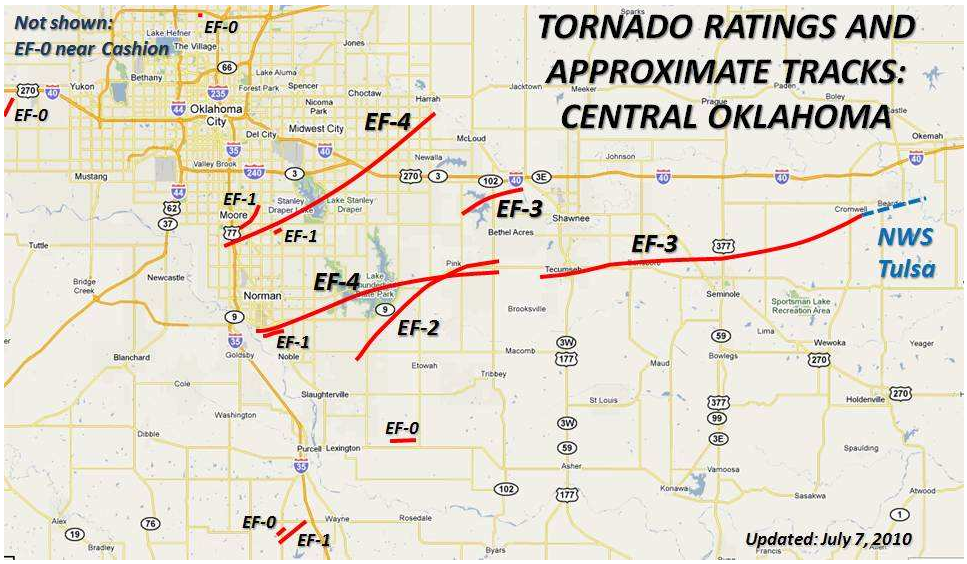

Figure 1: Damage paths of tornadoes near Oklahoma City on 10 May 2010 (Image courtesy of the Norman NWS WFO).

Many studies have documented the fine-scale structure of tornadoes using mobile radar observations (e.g., Bluestein et al., 1993; Bluestein and Crawford, 1997; Wurman and Gill, 2000; Bluestein et al., 2004; Alexander and Wurman, 2005; Bluestein et al., 2007; Wurman et al., 2007), which provided new information about tornado structure and helped validate laboratory and numerical model simulations. Wurman and Gill (2000) observed negative radial velocities in the center of the tornado, which they attributed to a downdraft in the center of the tornado between 400 m and the maximum height of their observations at 1 km. Other studies have used the ground-based velocity track display (GBVTD; Lee et al., 1999) to identify a two-cell vortex structure and associated axial downdraft (Lee and Wurman, 2005; Tanamachi et al., 2007; Kosiba and Wurman, 2010). Radar observations have also documented multiple vortex structure (e.g., Wurman, 2002), in addition to numerous visual accounts.

2.2. *Weak-echo hole and band structures around tornadoes*

A prominent signature in many tornadoes is a weak-echo hole (WEH), characterized by a reduction in reflectivity in the center of the tornado and higher reflectivity outside the core flow of the tornado (e.g., Fujita, 1981; Wakimoto and Martner, 1992; Wakimoto et al., 1996; Wurman and Gill, 2000; Bluestein et al., 2004; Wakimoto et al., 2011). Dowell et al. (2005) suspected that the WEH is caused by centrifuging of debris and hydrometeors within the center of the tornado, which reduces Z_{HH} in the center of the tornado. The WEH typically starts a few 100 m above the ground, with higher reflectivity below the WEH (e.g., Wurman and Gill, 2000; Bluestein et al., 2004; Wakimoto et al., 2011). Many studies have observed a ”U-shaped” WEH above this high reflectivity region (e.g., Wurman and Gill, 2000; Wakimoto et al., 2011), although Bluestein et al. (2004) documented a pear-shaped WEH.

Spiral bands are commonly observed within tornadoes, often with multiple bands within and surrounding the vortex (e.g., Fujita, 1981; Bluestein, 1993; Wurman et al., 1996; Wurman and Gill, 2000; Bluestein et al., 2003; Alexander and Wurman, 2005; Dowell et al., 2005; Bluestein et al., 2007). Wurman et al. (1996) and Wurman and Gill (2000) observed two spiral bands and suggested that the inner spiral band was composed of debris and the outer spiral band was composed of raindrops. Polarimetric observations by Bluestein et al. (2007) also revealed a double spiral band structure, and the polarimetric data showed that the inner and outer bands were composed of debris and raindrops, respectively.

3. DATA AND METHODOLOGY

OU-PRIME data from the 10 May 2010 outbreak are analyzed. For the technical detailed specifications for OU-PRIME, details about data collection on 10 May 2010, and an overview of the outbreak, the reader is referred to Palmer et al. (2011). OU-PRIME is a C-band, polarimetric radar with a 0.45° beamwidth and range resolution as fine as 25 m with oversampling, making it one of the highest resolution polarimetric radars in the world. OU-PRIME operates a 1-MW transmitter in a simultaneous transmit simultaneous receive (STSR) configuration, similar to the upgraded polarimetric Weather Surveillance Radar 1998

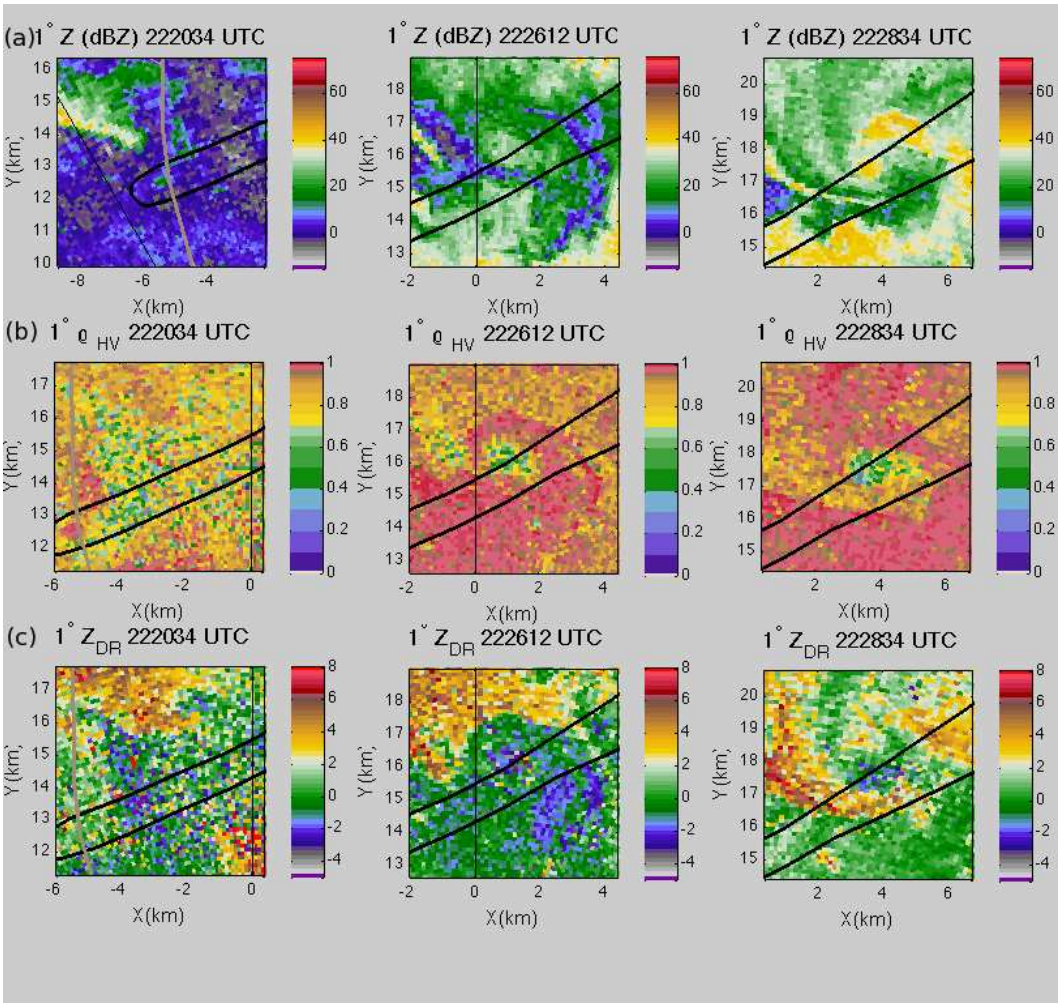

Figure 2: 1° PPI scans of (a) Z_{HH}, (b) ρ_{HV}, and (c) Z_{DR} at 2220, 2226, and 2228 UTC 10 May 2010. A TDS is not observed at 2220 UTC along the damage path, along some low ρ_{HV} values are observed. By 2226 UTC, a TDS is observed with reflectivity between 30 – 35 dBZ and ρ_{HV} below 0.6. As the tornado intensifies between 2226 – 2228 UTC, an increase in the areal extent of the TDS is observed.

Dopplers (WSR-88Ds; Doviak et al., 2000). The high transmit power provides very good sensitivity in clear-air regions.

On 10 May 2010, OU-PRIME was operated in a sector-scan mode to provide relatively rapid volumetric updates of 2 min 20 s – 2 min 40 s. The elevation angles included in the volume scan are 0.3°, 1°, 2°, 3°, 4°, 5°, 6.5°, and 9°. Data collection lasted from 1400 – 2331 UTC, with several tornadoes observed near the radar between 2220 – 2331 UTC. The radar operated a pulse length of 125 m, and a maximum unambiguous velocity of 16 m s^{-1}. Velocity data are subjectively unfolded using the National Center for Atmospheric Research's SOLO software (Oye et al., 1995)

During the 10 May 2010 tornado outbreak, 55 tornadoes struck portions of central and eastern Oklahoma. The two strongest tornadoes were rated EF-4 and occurred near Norman, Oklahoma (Fig. 1). This paper primarily focuses on EF-4 tornado that struck north Norman, Moore, and Oklahoma City. Smith et al. (2011) compare radar observations of this EF-4 tornado using multiple radars, and provide a broader discussion of velocity data. The EF-4 tornado that formed just east of the National Weather Center is discussed in detail by Bodine et al. (2010).

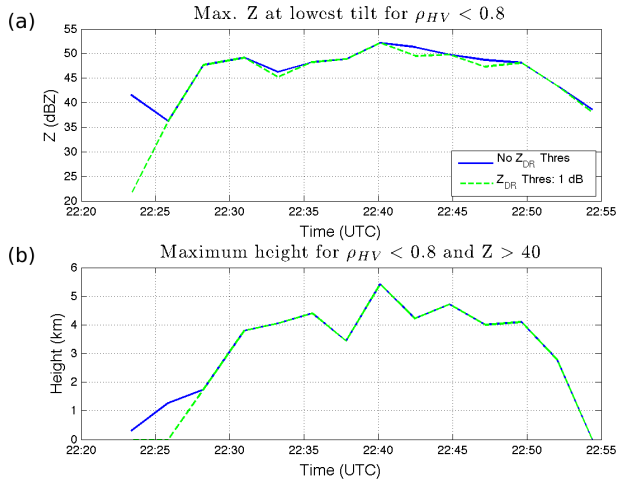

Figure 3: Time series of (a) $MAX\{Z_{HH}\}$ at the lowest tilt (1.0°) with $\hat{\rho}_{HV}$= 0.8, and (b) z_{max} for $\hat{\rho}_{HV}$= 0.8 and $\hat{Z}_{HH}$= 40 dBZ. Between 2226 – 2231 UTC, an increase in $MAX\{Z_{HH}\}$ and z_{max} are observed as the tornado intensifies and damage severity increases. As the tornado dissipates at 2251 UTC, both $MAX\{Z_{HH}\}$ and z_{max} decrease significantly. By 2254 UTC, the Z_{HH} falls below the reflectivity threshold and a TDS is no longer detected.

Ryzhkov et al. (2005) showed six parameters for the intensity of the TDS: the minimum and average ρ_{HV} value, minimum and average Z_{DR} value, and the number of pixels of $\rho_{HV} < 0.8$ and $Z_{DR} < 0.5$ dB. All of the parameters were examined at the lowest tilt. In the present study, we examine similar metrics for extreme values of ρ_{HV} and Z_{HH}, extend their application to all available tilts, and apply different threshold combinations. All parameters are computed within a 2-km radius of the center of the tornado. Large, wet hail can have very low ρ_{HV} values at C-band (Kumjian et al., 2010), which could create problems if hail and debris are located in close proximity. Hence, a sufficiently small search radius should be employed, particularly above the freezing level.

The parameter MAX$\{Z_{HH}\}$ is computed using two different methods which impose different thresholds on Z_{HH}. Z_{HH} should be higher during periods of more severe damage owing to a higher concentration of scatters and larger debris elements. Z_{HH} is typically higher at the lowest tilt since debris concentration and debris element size decrease as a function of height due to centrifuging (Dowell et al., 2005). The first method of determining MAX$\{Z_{HH}\}$ finds the maximum Z_{HH} where ρ_{HV} is below a ρ_{HV} threshold, $\hat{\rho}_{HV}$. For example, if $\hat{\rho}_{HV}$=0.7, then MAX$\{Z_{HH}\}$ corresponds to the maximum Z_{HH} value for range gates with $\rho_{HV} < 0.7$ within 2-km of the tornado center. The second method for MAX$\{Z_{HH}\}$ determines the maximum Z_{HH} where $\rho_{HV} < \hat{\rho}_{HV}$ and $Z_{DR} < \hat{Z}_{DR}$, where $\hat{Z}_{DR}$ is the Z_{DR} threshold. Another extrema-based TDS parameter is the minimum ρ_{HV}, or MIN$\{\rho_{HV}\}$, which is computed using a reflectivity threshold, $\hat{Z}_{HH}$. MIN$\{\rho_{HV}\}$ is also computed using both $Z_{HH} > \hat{Z}_{HH}$ and $Z_{DR} < \hat{Z}_{DR}$.

The second set of TDS parameters are based on spatial coverage of the TDS. The areal coverage of the TDS, A_{TDS}, provides an estimate of how much debris is being lofted at a particular elevation angle. A_{TDS} is defined as the total area (km^2) of range gates with $Z_{HH} > \hat{Z}_{HH}$ and $\rho_{HV} < \hat{\rho}_{HV}$. The volume of the TDS (1) is obtained by summing the areal coverage through all tilts in the volume scan after computing the representative depth of each tilt, ΔZ. If a debris signature is observed between two consecutive tilts, it is assumed to be continuous between the two tilts.

$$V(z) = \sum_{i=1}^{N} A_{TDS,i} \Delta Z \qquad (1)$$

The final TDS parameter is the maximum height of the debris column, z_{max}. z_{max} is the maximum height where $Z_{HH} > \hat{Z}_{HH}$ and $\rho_{HV} < \hat{\rho}_{HV}$. The maximum height is also computed by imposing an additional Z_{DR} threshold.

4. TORNADIC DEBRIS SIGNATURE

4.1. Temporal Evolution and TDS parameter performance

The primary use of the TDS has been tornado detection, so the performance of the TDS for tornado detection is briefly discussed. According to the NWS damage survey, the tornado formed at 2220 UTC in north Norman, just west of Indian Hills Road and I-35. The tornado caused mainly power line and tree damage along 1-35. A TDS is not observed at 2220 (Fig. 2) and 2223 UTC along the damage path, even though the radar measurements were about 300 m AGL. Although some regions of low ρ_{HV} are observed, very low Z_{HH} ($<$ 20 dBZ) suggests that the low ρ_{HV} values are associated with low SNR rather than tornadic debris. Hence, the tornado was not lofting sufficient debris to be detected. Between 2226 – 2252 UTC, a TDS was detected along the damage path of the tornado.

The tornado developed a clear tornado vortex signature (not shown) and a TDS at 2226 UTC (Fig. 2). The maximum reflectivity at 0.3° is 37 dBZ (Fig. 3a), and Z_{HH} remains relatively low throughout the TDS (30 – 37 dBZ). However, ρ_{HV} values between 0.4 – 0.7 and negative Z_{DR} (-1 to -3 dB) values are observed within the TDS. While tornadic debris typically has higher Z_{HH}, a developing or weak tornado may only loft light debris (e.g., dust, leaves). Hence, $\hat{Z}_{HH}$ for an initial tornado detection should be sufficiently low to detect light debris in weak or developing tornadoes. By 2228 UTC, the maximum radial velocity at 1.0° increases to 51.4 m s^{-1}. The TDS expands in areal coverage (Fig. 2), $MAX\{Z_{HH}\}$ exceeds 45 dBZ (Fig. 3a), and z_{max} increases to 1.7 km (Fig. 3b).

The tornado continues intensifying between 2228 – 2230 UTC with a maximum 1.0° radial velocity of 73.5 m s^{-1}at 2230 UTC. z_{max} increases from 47 to 49 dBZ (Fig. 3a) and $MAX\{Z_{HH}\}$ increases from 1.7 to 3.8 km AGL (Fig. 3b). At 2230 UTC, the tornado was located just west of Lake Stanley Draper. According to the Norman NWS WFO damage survey, the most severe damage occurred east of Lake Stanley Draper. So, the observations of increasing damage intensity as the tornado approached Lake Stanley Draper are consistent with the damage survey.

The Oklahoma City Police Department (OKCPD) provided a detailed damage survey within Oklahoma City, which indicates the degree of damage to homes (Fig. 4). A caveat is that the survey does not provide information about the type of housing unit or the construction of the home (hence, an EF-rating cannot be determined). At 2233 UTC, the tornado is located just east of Lake Stanley Draper, and caused some significant house damage (Fig. 4). By 2235 UTC, the tornado had passed through more residential areas, causing some major house damage and even destroying a few homes. Between 2231 – 2235 UTC, the TDS reaches the 9.0° tilt, so the maximum height of the debris signature cannot be determined. However, debris reached at least 3.8 – 4.5 km AGL during this period, indicating an intense updraft within the tornado and significant amounts of debris being ingested. The most severe damage occurred to the homes near 1-40 around 2237 UTC, and the EF-4 rating was determined from a home in the Deerfield West subdivision (located just west of the 2237 UTC marker in Fig. 4). The $MAX\{Z_{HH}\}$ parameter actually shows a slight decrease from the previous scan, although $MAX\{Z_{HH}\}$ still reaches 3.5 km AGL (Fig. 3b). Given that the parameter is based on the maximum height of a debris signature, the parameter will exhibit some lag since debris must be vertically advected to 3–5 km AGL. z_{max} approaches 50 dBZ at 2237 UTC, among the highest values observed during the tornado. The highest value of $MAX\{Z_{HH}\}$ during the tornado is observed at 2240 UTC, likely a combination of the peak tornado intensity and the high debris concentration after passing through the subdivision. The tornado continues to produce significant home damage during the 2240 – 2242 UTC scans, although the area affected is smaller compared to the 2237 UTC scan. $MAX\{Z_{HH}\}$ and z_{max} remain quite high during this period.

The tornado exits the OKCPD damage survey at 2242 UTC, so a detailed comparison of the TDS and debris is not possible from the OKCPD damage survey. The time of dissipation determined by the NWS damage survey was 2251 UTC. The updraft still lofts some debris at 2252 UTC. However, both $MAX\{Z_{HH}\}$ and z_{max} are decreasing significantly, indicating that the tornado is weakening or dissipating. Hence, even though the updraft may continue to loft debris during dissipation, the weakening or dissipation can still be observed by the falling debris column and lower Z_{HH} values. By 2254 UTC, a TDS is no longer observed.

An interesting observation is that the TDS is observed to the left of the damage track (Fig. 2). Storm motion of 25 – 30 m s^{-1} at about 240° resulted in much stronger ground-relative winds on the southeast side of the tornado. Such strong storm motion could result in differences of 50 – 60 m s^{-1} in tornado ground-relative winds. Hence, the greater damage severity along the southeast portion of the tornado is not surprising. Since the lowest radar observations in this study were about 300 – 500 m AGL, relating TDS aloft to a particular damage site would be difficult. To relate the TDS to a particular damage site, radar observations must be made very close to the ground since the debris is lofted and advected cyclonically. Although some heterogeneities are observed within the TDS, the TDS does not indicate more severe damage along the translational side of the tornado since the debris is transported away from its initial location.

4.2. Tornado Structure Revealed by Polarimetric Radar

The Moore-Oklahoma City EF-4 tornado exhibited interesting changes in vertical structure revealed by polarimetric radar. To observe larger-scale heterogeneities within the debris field, a centered, top-hat filter was applied to the data using a 3-by-3 rectangular window centered on the range gate. At 1° (about 420 m AGL), Z_{HH} is relatively uniform within the tornado, with a small difference of about 5 dB between the Z_{HH} minimum in the vortex center and outer debris field (Fig. 5a). However, some substantial differences are noted in ρ_{HV} and Z_{DR} between the vortex center and the outer debris field. ρ_{HV} (Fig. 5b) generally decreases as a function of range with the lowest values near the radius of maximum wind (RMW). Z_{DR} also decreases as a function of range with negative values (-1 to -3 dB) observed near the RMW compared to near-zero Z_{DR} near the vortex center (Fig. 5c). An interesting observation is that the regions of lowest Z_{DR} and ρ_{HV} tend to be collocated. Negative Z_{DR} values can result from Mie scattering (Ryzhkov et al., 2005), which would also cause low ρ_{HV} values. The negative Z_{DR} and very low ρ_{HV} regions may be regions of larger, centrifuged debris near the RMW, while near-zero Z_{DR} values and low ρ_{HV} values imply smaller debris element sizes near the vortex center. Very low ρ_{HV} values could also result from increased tumbling of debris within the stronger flow in the RMW. Another explanation for the negative Z_{DR} regions near the RMW is a common alignment among debris elements. While a common alignment among debris elements could result in negative Z_{DR} values, very low ρ_{HV} values suggest a low degree of alignment among debris elements. However, other contributions to very low ρ_{HV} could include the high dielectric constants of debris, irregular shapes, and large object sizes. Hence, some degree of common alignment among debris elements could not be ruled out.

A prominent WEH is observed in Z_{HH} at 2° (about 790 m AGL; Fig 5a). The difference in Z_{HH} between the vortex center and the outer debris ring is about 20 dB, indicating a substantial difference in debris concentration and/or size. Z_{DR} and ρ_{HV} exhibit similar trends to the 1° tilt, with Z_{DR} and ρ_{HV} decreasing as range increases from the vortex center (Fig 5b,c). The higher ρ_{HV} values within the vortex center may be explained by centrifuging of large debris elements and consequently, less variations in debris element size. Higher ρ_{HV} could also result from the presence of a strong axial updraft or downdraft, introducing some degree of common alignment among debris elements. Z_{HH} within the WEH continues to decreases at 3° (about 1.16 km AGL), decreasing to 20 dBZ in the vortex center. Z_{HH} values in the outer debris ring also decreased, particularly on the northern side. Northeast of the vortex center, a protrusion of higher ρ_{HV} (0.7 – 0.85) is observed wrapping into the vortex. The increase in ρ_{HV} could result from the entrainment of small drops from rain bands wrapping around the vortex.

5. SIMULATIONS OF PRECIPITATION EFFECTS ON THE TDS

The Moore-Oklahoma City EF-4 tornado was enshrouded by precipitation throughout its existence. Hence, the tornado likely entrained a substantial amount of precipitation, causing ρ_{HV} values to increase even though damage intensity was increasing. This effect on the TDS is best shown by examining the volume of debris gates (Fig. 6). If the TDS volume parameter were used to estimate tornado intensity, the tornado intensity would appear to decrease between 2233 – 2237 UTC when the tornado damage intensity was increasing to EF-3 and EF-4 intensity. Hence, the impact of precipitation on the TDS must be quantified for the spatial coverage metrics of the TDS to be an accurate indicator of tornado damage intensity when the tornado entrains precipitation. For this case, the extrema-based TDS parameters performed better than the spatial-coverage parameters due to precipitation effects.

The entrainment of precipitation to the TDS should lead to increased ρ_{HV} and higher Z_{DR} values. To simulate the effects of entraining precipitation into the TDS, raw time series (I/Q) data from within TDS are added to the raw time series data from precipitation. This experiment is performed for different Z_{HH} and Z_{DR} values to simulate the effects of adding different concentrations of rain drops, and different drop sizes. The signal powers of debris and precipitation are weighted by the reflectivity value within the range gate selected (i.e., if Z_{HH} for debris and precipitation are 50 dBZ and 40 dBZ, respectively, the amplitude of the debris signal is 10 times greater than the precipitation signal). Adding the two signals together doubles the noise, however both signals have high SNR which minimizes the additive noise impact. The simulations cannot account for interactions between precipitation and debris, such as water coating of debris, or complex scattering effects. Also, the time series signals from debris and precipitation are assumed to be independent. Moreover, the characteristics of precipitation within the tornado are much likely quite different from other regions of the storm. For example, the drop size distribution, and shapes and orientations of rain drops are probably much different within and near the tornado given the impact of stronger turbulence, horizontal and vertical wind shear, etc. Nonetheless, the experiment may be instructive for studying the impacts of precipitation on the TDS.

OU-PRIME data was thresholded based on Z_{HH}, ρ_{HV}, and Z_{DR} for debris, small drops, and large drops. Resolution volumes with debris (hereafter called debris volumes) were selected by identifying resolution volumes with $Z_{HH} \epsilon$ (40,50) dBZ, and $\rho_{HV} < 0.5$ within 2 km of the

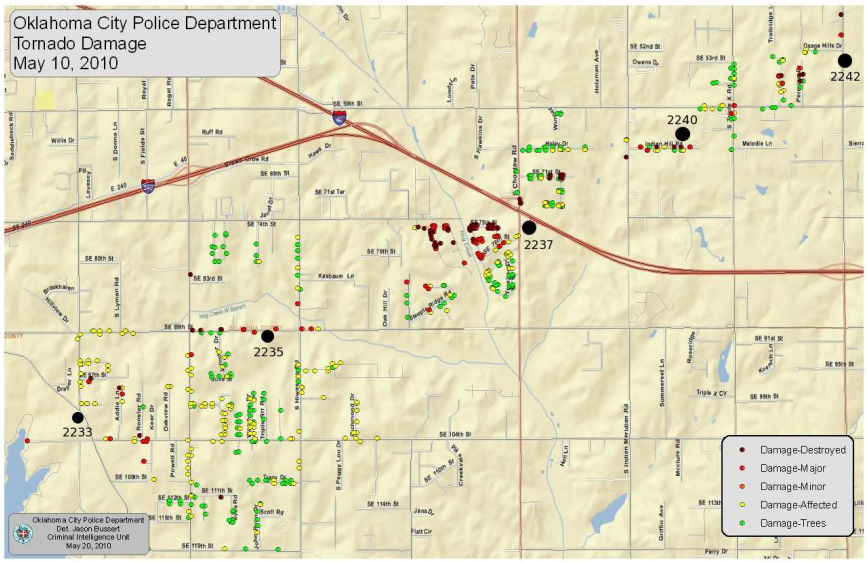

Figure 4: Damage survey provided by the Oklahoma City Police Department. Although an EF rating is not available, the damage survey provides an indication of the significance of the observed damage (Courtesy of the Oklahoma City Police Department). The position of the center of the tornado (from OU-PRIME) is labelled on the image with black dates and the scan time (UTC) is labelled in black.

tornado. For this experiment, OU-PRIME data at 22:30:58 UTC for May 10 was chosen because precipitation impacts on the TDS are minimal. Resolution volumes with small drops (hereafter called small drop volumes) were selected by identifying resolution volumes with $Z_{DR} \in$ (0.5,2) dB and $\rho_{HV} >$ 0.98. Finally, resolution volumes with large drops (hereafter called large drop volumes) were selected by identifying resolution volumes with $Z_{DR} \in$ (3,5) dB and $\rho_{HV} >$ 0.96. The small and large drop volumes were then sorted by Z_{HH} in the following ranges: 20 – 30, 30 – 40, 40 – 50, and 50 – 60 dBZ. This provides a total of 8 sets of resolution volumes, with 4 small drop and 4 large drop sets for the 4 Z_{HH} ranges.

For each precipitation case, a resolution volume was randomly selected that met the criteria for the desired drop size distribution (i.e., small or large drop volumes) and the desired reflectivity range. To simulate the effects of precipitation and debris within the same resolution volume, the time series data from the precipitation resolution volume is added to time series data from a randomly selected debris volume. After adding the time series signals for the small/large drop volumes and debris, ρ_{HV} and Z_{DR} are recomputed to provide estimates for the mixed volume. This process was repeated 100 times to determine mean ρ_{HV} and Z_{DR} values for the mixed volumes.

Tables 1 and 2 shows the mean values of Z_{DR} and ρ_{HV} for debris, precipitation, and a mixed volume of debris and precipitation. For all cases, the Z_{HH} from the debris

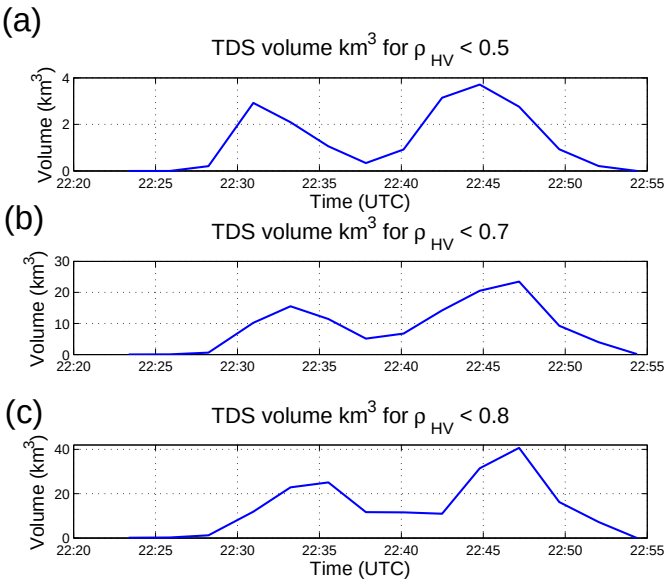

Figure 6: TDS volume with $\hat{\rho}_{HV}$ of (a) 0.5, (b) 0.7, and (c) 0.8.

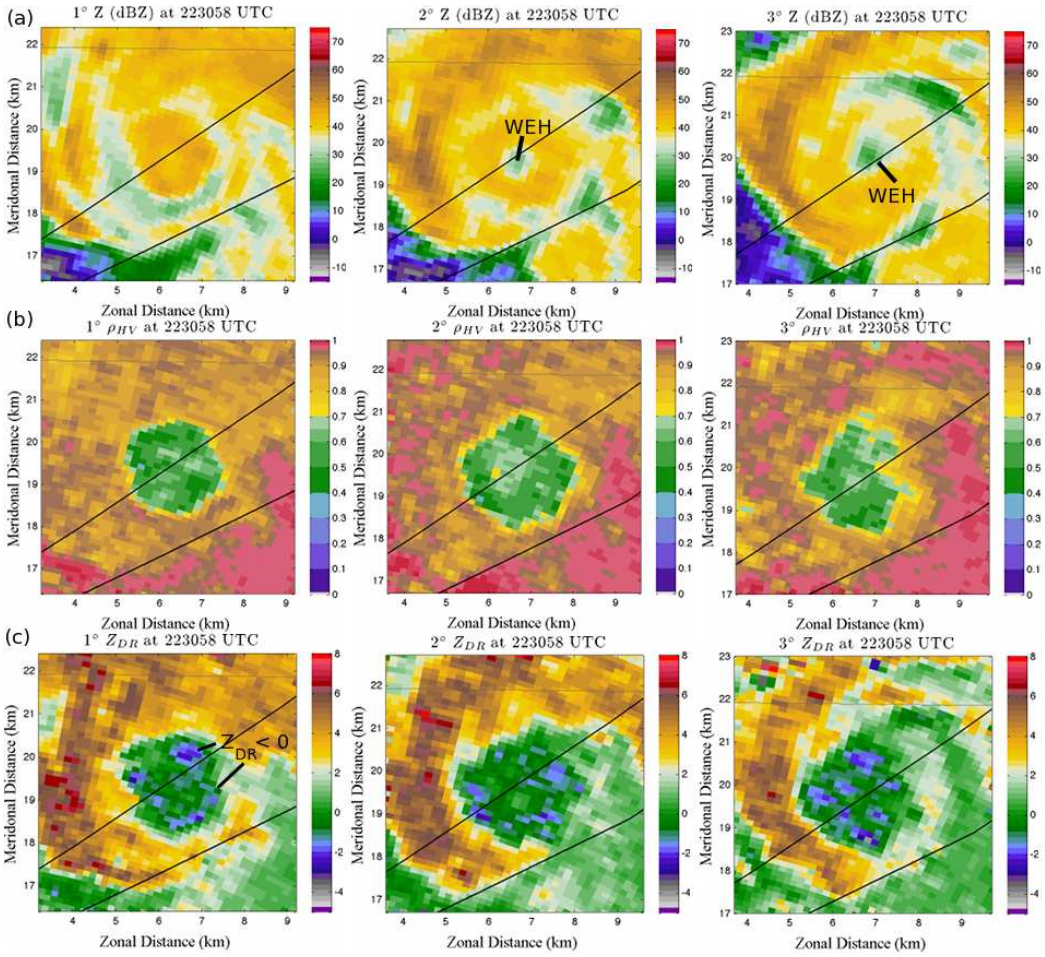

Figure 5: Filtered 1°, 2°, and 3° (a) Z_{HH}, (b) ρ_{HV}, and (c) Z_{DR} at 2230 UTC 10 May 2010. The location of the weak-echo hole (WEH) is annotated on (a), and the location of some low Z_{DR} regions within the TDS are shown at 1°. In general, negative Z_{DR} values and low ρ_{HV} values were found near the radius of maximum wind.

Table 1: Mean Z_{DR} values for different precipitation, debris, and mixed volumes. In all cases, Z_{HH} for the debris volumes was 40 – 50 dBZ. The first two columns, precip Z_{HH} and precip Z_{DR} describe the range of Z_{HH} and Z_{DR} values for the precipitation volumes. $\overline{Z_{DR}}$ Mixed is the mean Z_{DR} value for 100 combined volumes of debris and precipitation for the stated Z_{HH} and Z_{DR} ranges. $\overline{\Delta Z_{DR}}$ is the mean Z_{DR} change resulting from adding precipitation to the debris volume.

Precip Z_{HH}	Precip Z_{DR}	$\overline{Z_{DR}}$ Debris	$\overline{Z_{DR}}$ Precip	$\overline{Z_{DR}}$ Mixed	$\overline{\Delta Z_{DR}}$
(20,30)	(0.5,2)	-0.32	1.11	-0.28	0.04
(20,30)	(4,6)	-0.30	4.76	-0.28	0.02
(30,40)	(0.5,2)	-0.32	1.01	-0.04	0.28
(30,40)	(4,6)	-0.23	5.05	-0.08	0.15
(40,50)	(0.5,2)	-0.50	1.21	-0.44	0.06
(40,50)	(4,6)	-0.34	5.03	0.91	1.25
(50,60)	(0.5,2)	-0.45	1.63	1.22	1.67
(50,60)	(4,6)	-0.52	4.96	2.78	3.30

Table 2: Mean ρ_{HV} values for different precipitation, debris, and mixed volumes. In all cases, Z_{HH} for the debris volumes was 40 – 50 dBZ. The first two columns, precip Z_{HH} and precip Z_{DR} describe the range of Z_{HH} and Z_{DR} values for the precipitation volumes. $\overline{\rho_{HV}}$ Mixed is the mean ρ_{HV} value for 100 combined volumes of debris and precipitation for the stated Z_{HH} and Z_{DR} ranges. $\overline{\Delta\rho_{HV}}$ is the mean ρ_{HV} change resulting from adding precipitation to the debris volume.

Precip Z_{HH}	Precip Z_{DR}	$\overline{\rho_{HV}}$ Debris	$\overline{\rho_{HV}}$ Precip	$\overline{\rho_{HV}}$ Mixed	$\overline{\Delta\rho_{HV}}$
(20,30)	(0.5,2)	0.409	0.987	0.462	0.05
(20,30)	(4,6)	0.402	0.973	0.403	0.00
(30,40)	(0.5,2)	0.407	0.986	0.509	0.10
(30,40)	(4,6)	0.408	0.974	0.413	0.01
(40,50)	(0.5,2)	0.410	0.987	0.668	0.26
(40,50)	(4,6)	0.410	0.973	0.496	0.09
(50,60)	(0.5,2)	0.412	0.983	0.819	0.41
(50,60)	(4,6)	0.415	0.973	0.692	0.28

resolution volumes was between 40–50 dBZ. For both small and large drop volumes with low Z_{HH} (20 – 30 dBZ), adding precipitation to the debris resolution volume results in very small changes in Z_{DR}. For ρ_{HV}, the small drops have a greater impact on ρ_{HV} value for the mixed resolution volume compared to the large drops. For small and large drop volumes with Z_{HH} between 30 – 40 dBZ or 10 dB lower than the debris volume, adding precipitation to the debris volume increases Z_{DR} by 0.23 and 0.15 dB for small and large drops volumes, respectively. Again, a larger increase in ρ_{HV} is observed for small drops compared to large drops. When Z_{HH} of the precipitation volume and debris volume are both 40 – 50 dBZ, mean ρ_{HV} for small and large drops increases by 0.26 and 0.09, respectively. The mean Z_{DR} change for large drops becomes significant, increasing by 1.25 dB. When Z_{HH} of the precipitation volume is 50 – 60 dBZ, very large increases in ρ_{HV} are observed. For both cases, large increases in Z_{DR} are observed in the mixed volume compared to the debris volume.

Some open questions emerge about the impact of precipitation on the TDS, and the utility of the TDS parameters in heavy precipitation. First, given that the characteristics of precipitation in the environment surrounding the tornado can be identified using polarimetric data, can the potential bias on the TDS be quantified and corrected? While the TDS may provide a good indicator of damage or tornado intensity in the absence of precipitation, the entrainment precipitation will increase ρ_{HV} and Z_{DR}, and result in an underestimate of the tornado strength or debris volume. At a minimum, the capability to identify precipitation entrainment and its potential impact would be useful to provide a measure of the TDS parameters accuracy. A possible method of correction could be adjusting the ρ_{HV} and Z_{DR} thresholds to account for the higher ρ_{HV} and Z_{DR} observed in entrainment cases.

6. CONCLUSIONS

This paper investigates the potential of using TDS parameters for determining tornado damage intensity. Several TDS parameters were tested on polarimetric data from OU-PRIME on Moore-Oklahoma City EF-4 tornado on 10 May 2010. The results show that the TDS parameters have the potential to assess tornado damage intensity, consistent with previous results by Ryzhkov et al. (2005). In the present study, we examine the performance of two new TDS parameters: the maximum height of the debris column, $MAX\{Z_{HH}\}$, and maximum reflectivity at the lowest tilt, z_{max}. These TDS parameters showed good overall agreement with tornado intensity and the severity of damage. In particular, very good agreement between these TDS parameters and observed damage was seen during the intensification and dissipation phases of the tornado. The intensification of the tornado corresponds to a rapid increase in $MAX\{Z_{HH}\}$ and z_{max}, and the dissipation of the tornado corresponds to a rapid decrease in $MAX\{Z_{HH}\}$ and z_{max}. For this case, the Z_{DR} threshold for the $MAX\{Z_{HH}\}$ and z_{max} parameters had little impact since Z_{DR} values within the tornado were mainly below 1 dB. In contrast, the spatial parameters for the areal and volumetric coverage of the TDS did not perform well during periods of precipitation entrainment.

The structure of the Moore-Oklahoma City EF-4 tornado changed dramatically within the lowest 1.1 km AGL. At 420 m AGL, Z_{HH} was relatively uniform throughout the TDS. However, ρ_{HV} and Z_{DR} decreased as a function of range, reaching a minimum near the RMW. Negative Z_{DR} and very low ρ_{HV} values tended to be collocated, which suggests either large debris element sizes or decreased alignment of debris elements (e.g., increased tumbling in stronger flow). Given that the largest debris elements are centrifuged more

quickly than small debris elements (e.g., Dowell et al., 2005), such observations could indicate a radial dependence in debris element size due to centrifuging. The WEH observed in previous studies typically formed within the lowest 300 – 400 m AGL (e.g., Wurman and Gill, 2000; Bluestein et al., 2004; Wakimoto et al., 2011). Wakimoto et al. (2011) observed a WEH forming within the 300 – 400 m of the surface whereas the lowest observation of the WEH in the present study is at 790 m AGL. Given that the diameter of the the Moore-Oklahoma City tornado was approximately about 2 km wide compared to the 200–300 m diameter LaGrange, Wyoming tornado examined by Wakimoto et al. (2011), differences in centrifugal forces may account for the differences in WEH height. For the same tangential wind speed, a tornado with a smaller diameter will have stronger centrifugal forces. Although the winds within the Moore-Oklahoma City tornado were 10 m s^{-1} stronger than the LaGrange tornado, the impact of the smaller tornado diameter is more significant. Hence, the weaker centrifuging within the Moore-Oklahoma City tornado might account for the higher height of the WEH observed in the present case.

Time series simulations of mixed volumes of debris and precipitation showed that entraining precipitation into the TDS will cause an increase in Z_{DR} and ρ_{HV}. The 10 May 2010 tornado was consistently surrounded by precipitation throughout its duration. During the period when the most intense damage was observed, the spatial coverage of low ρ_{HV} values actually decreased. Hence, the impact of precipitation entrainment on the TDS must be quantified, and methods of accounting for precipitation entrainment should be developed. A simple solution includes increasing the ρ_{HV} and Z_{DR} thresholds if precipitation entrainment is suspected. However, increasing the ρ_{HV} and Z_{DR} thresholds could introduce errors in the TDS parameters by including range gates where tornadic debris is not present (e.g., hail).

The TDS parameters are currently being tested on other tornadoes from the 10 May 2010 and 24 May 2011 tornado outbreaks. An examination of multiple tornado cases should provide information about how well the TDS can assess overall damage intensity (e.g., can TDS parameters discriminate between weak, strong, and violent tornadoes?). Moreover, multiple tornado cases may also reveal how sensitive the TDS parameters are to external factors that influence the TDS (other than tornado intensity), variations in the concentration or type of manmade structures (e.g., population density), or changes in vegetation. Future plans also include implementing the TDS parameters on KOUN polarimetric data to assess the performance of the TDS parameters on the operational polarimetric WSR-88D network. The TDS parameters could provide a valuable tool for forecasters if real-time information about tornado intensity can be extracted from polarimetric radar.

7. ACKNOWLEDGMENTS

The authors thank the administration of the University of Oklahoma (OU), which supported the development of OU-PRIME and other facilities at OU. OU-PRIME is maintained and operated by OU's Atmospheric Radar Research Center (ARRC) and the authors appreciate the efforts of Redmond Kelley, Boon Leng Cheong, and others who helped maintain the radar. The authors greatly appreciate the damage surveys provided by Doug Speheger, Greg Stumpf, and Gabe Garfield. The details provided in these damage surveys were critical for making comparisons between the observed damage and radar observations. Discussions with Chris Schwarz, Daniel Betten, Conrad Ziegler, and Doug Speheger were also helpful.

References

Alexander, C. R., and J. Wurman, 2005: The 30 May 1998 Spencer, South Dakota storm. Part I: The structural evolution and environment of the tornadoes. *Mon. Wea. Rev.*, **133**, 72–96.

Bluestein, H. B., 1993: *Synoptic-Dynamic Meteorology in Midlatitudes*. Vol. 2. Oxford University Press.

Bluestein, H. B., and T. M. Crawford, 1997: Mesoscale dynamics of the near-dryline environment: Analysis of data from COPS-91. *Mon. Wea. Rev.*, **121**, 1354–1372.

Bluestein, H. B., M. M. French, R. L. Tanamachi, S. Frasier, K. Hardwick, F. Junyent, and A. Pazmany, 2007: Close-range observations of tornadoes in supercells made with a dual-polarization, X-band, mobile Doppler radar. *Mon. Wea. Rev.*, **135**, 1522–1543.

Bluestein, H. B., J. G. LaDue, H. Stein, D. Spegher, and W. P. Unruh, 1993: Doppler radar wind spectra of supercell tornadoes. *Mon. Wea. Rev.*, **121**, 2200–2221.

Bluestein, H. B., C. C. Weiss, and A. L. Pazmany, 2003: Mobile Doppler radar observations of a tornado in a supercell near Bassett, Nebraska, on 5 June 1999. Part I: Tornadogenesis. *Mon. Wea. Rev.*, **131**, 2954–2967.

Bluestein, H. B., C. C. Weiss, and A. L. Pazmany, 2004: The vertical structure of a tornado near Happy, Texas, on 5 May 2002: High-resolution, mobile, W-band, Doppler radar observations. *Mon. Wea. Rev.*, **132**, 2325–2337.

Bodine, D., R. D. Palmer, M. R. Kumjian, and A. V. Ryzhkov, 2010: High-resolution OU-PRIME radar observations of a prolific tornado-producing supercell on 10 May 2010. in Amer. Meteor. Soc., editor, *25th Conf. on Severe Local Storms*, Denver, CO.

Church, C., D. Burgess, C. Doswell, and R. Davies-Jones, Eds., 1993: *The Tornado: Its Structure, Dynamics, Prediction and Hazards*. Amer. Geophys Union.

Church, C. R., and J. T. Snow, 1993: Laboratory models of tornadoes. in *The Tornado: Its Structure, Dynamics, Prediction and Hazards*, No. 79, pp. 19–39. Amer. Geophys Union.

Church, C. R., J. T. Snow, G. L. Baker, and E. M. Agee, 1979: Characteristics of tornado-like vortices as a function of swirl ratio: A laboratory investigation. *J. Atmos. Sci.*, **36**, 1755–1776.

Davies-Jones, R., R. J. Trapp, and H. B. Bluestein, 2001: Tornadoes and tornadic storms. in C. A. Doswell, editor, *Severe Convective Storms*, pp. 167–222. Amer. Meteor. Soc.

Davies-Jones, R. P., 1973: The dependence of core radius on swirl ratio in a tornado simulator. *J. Atmos. Sci.*, **30**, 1427–1430.

Davies-Jones, R. P., 1986: Tornado dynamics. in E. Kessler, editor, *Thunderstorm Morphology and Dynamics*, pp. 197–236. University of Oklahoma Press, 2d. edition.

Doviak, R. J., V. Bringi, A. Ryzhkov, A. Zahrai, and D. Zrnić, 2000: Considerations for polarimetric upgrades to operational WSR-88D radars. *J. Atmos. Oceanic Technol.*, **17**, 257 – 278.

Dowell, D. C., C. R. Alexander, J. M. Wurman, and L. J. Wicker, 2005: Centrifuging of hydrometeors and debris in tornadoes: Radar-reflectivity patterns and wind-measurement errors. *Mon. Wea. Rev.*, **133**, 1501–1524.

Fujita, T. T., 1981: Tornadoes and downbursts in the context of generalized planetary scales. *J. Atmos. Sci.*, **38**, 1511–1534.

Kosiba, K., and J. Wurman, 2010: The three-dimensional axisymmetric wind field structure of the Spencer, South Dakota, 1998 tornado. *J. Atmos. Sci.*, **67**, 3074–3083.

Kumjian, M. R., J. C. Picca, S. M. Ganson, A. V. Ryzhkov, and J. Krause, 2010: Polarimetric radar characteristics of large hail. in Amer. Meteor. Soc., editor, *25th Conf. on Severe Local Storms*, Denver, CO.

Kumjian, M. R., and A. V. Ryzhkov, 2008: Polarimetric signatures in supercell thunderstorms. *J. Appl. Meteor. Climatol.*, **48**, 1940–1961.

Lee, W. C., B. J.-D. Jou, P.-L. Chang, and S.-M. Deng, 1999: Tropical cyclone kinematic structure retrieved from single-Doppler radar observations. Part I: Doppler velocity patterns and the GBVTD technique. *Mon. Wea. Rev.*, **127**, 2419–2439.

Lee, W.-C., and J. Wurman, 2005: Diagnosed three-dimensional axisymmetric structure of the Mulhall tornado on 3 May 1999. *J. Atmos. Sci.*, **62**, 2373–2393.

Oye, R. C., K. Mueller, and S. Smith, 1995: Software for radar translation, editing, and interpolation. in *Preprints, 27th Conf. on Radar Meteorology*, pp. 359–361, Vail, CO. Amer. Meteor. Soc.

Palmer, R. D., D. Bodine, M. Kumjian, B. Cheong, G. Zhang, Q. Cao, H. B. Bluestein, A. Ryzkhov, T.-Y. Yu, and Y. Wang, 2011: The 10 May 2010 tornado outbreak in central Oklahoma: Potential for new science with high-resolution polarimetric radar. *Bull. Amer. Meteor. Sci.*, **92**, 871–891.

Rotunno, R., 1977: Numerical simulation of a laboratory vortex. *J. Atmos. Sci.*, **34**, 1942–1956.

Rotunno, R., 1979: A study in tornado-like vortex dynamics. *J. Atmos. Sci.*, **36**, 140–155.

Rotunno, R., 1984: An investigation of a three-dimensional asymmetric vortex. *J. Atmos. Sci.*, **41**, 283–298.

Rotunno, R., 1986: Tornadoes and tornadogenesis. in P. Ray, editor, *Mesoscale Meteorology and Forecasting*, pp. 414–436. Amer. Meteor. Soc.

Ryzhkov, A. V., T. J. Schuur, D. W. Burgess, P. L. Heinselman, S. E. Giangrande, and D. S. Zrnić, 2005: The joint polarization experiment: Polarmetric rainfall measurements and hydrometeor classification. *Bull. Amer. Meteor. Sci.*, **86**, 809–824.

Ryzkhov, A., D. Burgess, D. Zrnić, T. Smith, and S. Giangrande, 2002: Polarimetric analysis of a 3 May 1999 tornado. in Amer. Meteor. Soc., editor, *Preprints, 22th Conf. on Severe Local Storms*, Hyannis, MA.

Smith, A. J., D. Bodine, P. L. Heinselman, and P. B. Chilson, 2011: Using velocity data from nwrt par and ou-prime to determine dynamics affecting rapid intensification of an ef4 tornado. in Amer. Meteor. Soc., editor, *35th Conf. on Radar Meteorology*, Pittsburgh, PA.

Tanamachi, R. L., H. B. Bluestein, W. C. Lee, M. Bell, and A. L. Pazmany, 2007: Ground-based velocity track display (gbvtd) analysis of W-band radar data in a tornado near Stockton, Kansas on 15 May 1999. *Mon. Wea. Rev.*, **135**, 783–800.

Wakimoto, R. M., N. T. Atkins, and J. Wurman, 2011: The LaGrange tornado during VORTEX2. Part I: Photogrammetric analysis of the tornado combined with single-doppler radar data. *Mon. Wea. Rev.*, **submitted**.

Wakimoto, R. M., W.-C. Lee, H. B. Bluestein, C.-H. Liu, and P. H. Hildebrand, 1996: ELDORA observations during VORTEX 95. *Bull. Amer. Meteor. Sci.*, **77**, 1465–1481.

Wakimoto, R. M., and B. E. Martner, 1992: Observations of a Colorado tornado. Part II: Combined photogrammetric and Doppler radar analysis. *Mon. Wea. Rev.*, **120**, 522–543.

Ward, N. B., 1972: The exploration of certain features of tornado dynamics using a laboratory model. *J. Atmos. Sci.*, **29**, 1194–1204.

Wurman, J., 2002: The multiple-vortex structure of a tornado. *Wea. Forecasting*, **17**, 473–505.

Wurman, J., and S. Gill, 2000: Finescale radar observations of the Dimmitt, Texas (2 June 1995), tornado. *Mon. Wea. Rev.*, **128**, 2135–2164.

Wurman, J., Y. Richardson, C. Alexander, S. Weygandt, and P.-F. Zhang, 2007: Dual-doppler and single-doppler analysis of a tornadic storm undergoing mergers and repeated tornadogenesis. *Mon. Wea. Rev.*, **135**, 736–758.

Wurman, J., J. M. Straka, and E. N. Rasmussen, 1996: Fine-scale Doppler radar observations of tornadoes. *Science*, **272**, 1774–1777.

Zrnić, D. S., and A. V. Ryzhkov, 1999: Polarimetry for weather surveillance radars. *Bull. Amer. Meteor. Sci.*, **80**, 389–406.